Journal of Biomechanics 88 (2019) 55–63

Contents lists available at ScienceDirect

Journal of Biomechanics

journal homepage: www.elsevier.com/locate/jbiomech
www.JBiomech.com

Development of a statistical shape-function model of the implanted knee for real-time prediction of joint mechanics

Kalin D. Gibbons [a], Chadd W. Clary [b], Paul J. Rullkoetter [b], Clare K. Fitzpatrick [a,*]

[a] Computational Biosciences Laboratory, Mechanical and Biomedical Engineering, Boise State University, Boise, ID, United States
[b] Center for Orthopaedic Biomechanics, University of Denver, Denver, CO, United States

ARTICLE INFO

Article history:
Accepted 10 March 2019

Keywords:
Total knee arthroplasty
Finite element analysis
Statistical shape model
Joint mechanics
Real-time prediction

ABSTRACT

Outcomes of total knee arthroplasty (TKA) are dependent on surgical technique, patient variability, and implant design. Non-optimal design or alignment choices may result in undesirable contact mechanics and joint kinematics, including poor joint alignment, instability, and reduced range of motion. Implant design and surgical alignment are modifiable factors with potential to improve patient outcomes, and there is a need for robust implant designs that can accommodate patient variability. Our objective was to develop a statistical shape-function model (SFM) of a posterior stabilized implanted knee to instantaneously predict joint mechanics in an efficient manner. Finite element methods were combined with Latin hypercube sampling and regression analyses to produce modeling equations relating nine implant design and six surgical alignment parameters to tibiofemoral (TF) joint mechanics outcomes during a deep knee bend. A SFM was developed and TF contact mechanics, kinematics, and soft tissue loads were instantaneously predicted from the model. Average normalized root-mean-square error predictions were between 2.79% and 9.42%, depending on the number of parameters included in the model. The statistical shape-function model generated instantaneous joint mechanics predictions using a maximum of 130 training simulations, making it ideally suited for integration into a patient-specific design and alignment optimization pipeline. Such a tool may be used to optimize kinematic function to achieve more natural motion or minimize implant wear, and may aid the engineering and clinical communities in improving patient satisfaction and surgical outcomes.

1. Introduction

Outcomes of total knee arthroplasty (TKA) are dependent on surgical technique, patient variability, and implant design. Non-optimal design or alignment choices may result in undesirable contact mechanics and joint kinematics, including poor alignment, instability, and reduced range of motion. Some of the concerns specifically affecting posterior stabilized designs are bone resection, cam position, post wear and breakage, patellar clunk, and anterior-posterior (A-P) mid flexion instability (Scuderi et al., 2012). Patient satisfaction rates range from 75% to 92%, with primary complaints being residual pain and limited function, including difficulty kneeling, squatting, and climbing stairs after TKA, resulting in only 22% of patients rating their surgical outcomes as 'excellent' (Choi and Ra, 2016). Implant design and surgical alignment are modifiable factors that have potential to improve patient outcomes. There is a need for robust implant designs that can accommodate patient-specific sources of variability. Real-time prediction of TKA joint mechanics under variable design and/or alignment conditions would facilitate incorporating these factors into patient-specific surgical planning strategies to optimize post-operative joint mechanics.

Prior research has assessed joint mechanics outcomes for TKA procedures both experimentally and computationally, with FE methods used extensively in both deterministic and probabilistic studies using available patient data, as well as data generated through statistical means (Galloway et al., 2012). Studies focusing on implant design (Willing and Kim, 2011), surgical decisions (Kessler et al., 2008; Thompson et al., 2011), and subject-specific factors (Elias et al., 2010; Dhaher and Kahn, 2002; Mesfar and Shirazi-Adl, 2005) have been conducted, while other work has quantified the relative contributions of each source with respect to total variability (Fitzpatrick et al., 2012). Recent work has identified geometric parameters of the articular surface that cause a competing duality between optimal contact pressure and knee kinematics (Ardestani et al., 2015). The authors noted that femoral

* Corresponding author at: Mechanical and Biomedical Engineering, Boise State University, 1910 University Drive, MS-2085, Boise, ID 83725-2085, United States.
E-mail address: clarefitzpatrick@boisestate.edu (C.K. Fitzpatrick).

https://doi.org/10.1016/j.jbiomech.2019.03.010
0021-9290/

and tibial distal radii, femoral and tibial posterior radii, and femoral coronal radius were all parameters that affected contact mechanics and kinematics simultaneously, and gave pairs of parameters that would optimize either contact pressure or knee kinematics at minimal detriment to the other.

While these past efforts have given valuable insight into predicting surgical outcomes following TKA, there are inefficiencies that limit their usefulness to individual patients within the clinical setting. In vitro experiments are often expensive, which limits the number of designs or alignments that may feasibly be evaluated. Finite element (FE) methods combined with probabilistic analysis provides an effective platform to investigate coupled interactions between knee design parameters, surgical choices, and patient-specific variability (Ardestani et al., 2015). However, time, effort, and expertise is required to perform each simulation, which imposes a barrier to adoption of traditional FE methods for development of targeted TKA treatments on a patient-specific basis. A statistical model linking design and alignment parameters to joint mechanics outcomes with real-time response could have substantial utility during surgical planning to guide the optimal surgical choices for an individual.

Our objective was the development of a statistical shape-function model (SFM) of a posterior stabilized implanted knee to instantaneously predict output mechanics in a resource efficient manner. Finite element methods were combined with Latin hypercube sampling (LHS) and regression analysis to produce modeling equations relating nine implant design and six surgical alignment parameters to tibiofemoral (TF) joint mechanics outcomes during a deep knee bend (DKB) activity. Initially, only design parameters were modified and resulting TF contact mechanics, kinematics, and soft tissue loads were predicted. Once the initial prediction algorithms were tuned, a separate set of models with averaged design parameters and varied surgical parameters were developed. Finally, a SFM was developed where both design and surgical parameters were varied, and joint mechanics were instantaneously predicted from the resulting model.

2. Methods

The FE model in this study was based on a previously developed model of an implanted posterior-stabilized (PS) knee (Fitzpatrick et al., 2012, 2014). In brief, the model consisted of femoral, tibial, and patellar bones and implants, patellar tendon, quadriceps, and PF and TF ligaments (Fig. 1). Each ligament was represented by non-linear tension-only spring elements, with reference strains and linear stiffness parameters adopted from prior work (Baldwin et al., 2012). Ligaments included medial and lateral collateral ligaments (MCL, LCL--separated into anterior, medial and posterior bundles), anterior lateral capsule (ALC), popliteofibular ligament (PFL), posteromedial capsule (PMC), medial and lateral posterior capsule (MCAP, LCAP), and medial and lateral posterior oblique structures (MPOL, LPOL). The quadriceps muscle, which was separated into rectus femoris plus vastus intermedius (RF + VI), vastus lateralis (VL) and vastus medialis (VM) bundles, was represented by two-dimensional (2-D) fiber-reinforced membrane elements to allow for contact and wrapping in deep flexion, with line of action for each bundle based on cadaveric data (Farahmand et al., 2004). Sensors in the FE model, represented using connector elements, were used to connect each tibial implant surface (separated into medial, lateral and post components) to the underlying tibial bone. These sensors were used to record the 6-DOF loads acting on each surface. Bone and components were modeled as rigid bodies, for computational efficiency, with contact between the components defined using a pressure-overclosure relationship (Halloran et al., 2005). A coefficient

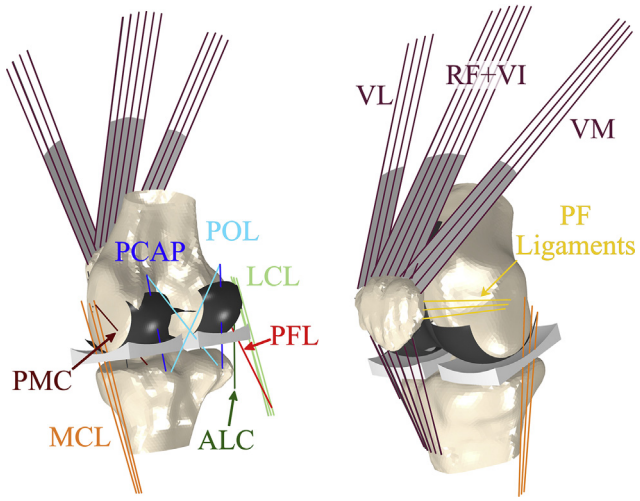

Fig. 1. Finite element model of implanted knee joint. Ligaments modeled in this simulation included medial and lateral collateral ligaments (MCL, LCL), anterior lateral capsule (ALC), popliteofibular ligament (PFL), postero-medial capsule (PMC), posterior capsule (PCAP), and posterior oblique structures (POL). The quadriceps muscle, which was separated into rectus femoris plus vastus intermedius (RF + VI), vastus lateralis (VL) and vastus medialis (VM) bundles, was represented by 2-D fiber-reinforced membrane elements. Patellofemoral ligaments and patellar ligament (PL) were also included.

of friction between the femoral component and polyethylene components of 0.04 was applied (Godest et al., 2002; Hashemi and Shirazi-Adl, 2000).

Knee loads and muscle forces were applied using hinge, translational, or cylindrical (allowing both rotation and translation) mechanical actuators, implemented in our FE simulations through force- or moment-driven connector elements. To create a 6-DOF TF joint, quadriceps load was applied to the RF + VI, VL and VM actuators, vertical load was applied at the hip, anterior-posterior (A-P) force was applied to the femur, with femoral internal-external (I-E) rotation constrained, medial-lateral (M-L) translation free, and knee flexion determined by a balance of vertical hip and quadriceps load. I-E and varus-valgus (V-V) torques were applied to the tibia, with the remaining tibial DOFs constrained. The patella was kinematically unconstrained in all 6-DOF, with constraint provided by the patellar ligament (PL), patellofemoral ligaments, and quadriceps (Baldwin et al., 2012).

The knee flexion profile for a deep knee bend simulation was adopted from video recordings of five patients with telemetric implants during a knee bend activity (Heinlein et al., 2007; Kutzner et al., 2010). TF compression, A-P, I-E and V-V loading profiles were extracted from the published telemetric data of these same patients. Flexion and joint loading profiles were averaged across the five subjects to create representative TKA profiles. These were used as load and kinematic targets in the FE simulation. Sensors in the FE model were used to measure knee flexion angle, compressive, A-P, I-E, and V-V loads at the tibiofemoral joint throughout the dynamic knee flexion simulation where the knee was flexed from full extension to 100° flexion. A proportional-integral (PI) control system was implemented in the model through an Abaqus/Explicit user subroutine to apply the external loads required to match the target joint loading and flexion profiles. External loads were applied through translational and rotational connectors to apply a vertical load to the hip, A-P force to the femur, I-E and V-V torques to the tibia, and muscle forces to the quadriceps. The quadriceps force was updated via the control system to match flexion angle, while loads in the vertical hip, femoral A-P, tibial I-E and tibial V-V connectors were updated to match their associated TF joint loading profile.

Implant geometry was parameterized using nine variables: femoral condyle distal, posterior and coronal radii, tibial insert anterior, posterior and coronal plane conformity, trochlear orientation and M-L position, and coronal plane curvature of the cam mechanism (Fig. 2). Ranges of design parameters were based on the geometric range of commercially available TKA components. Six surgical alignment predictors included: tibial insert and femoral implant V-V and I-E alignment, femoral F-E alignment, and tibial insert slope, with ranges chosen to capture those of both mechanically and kinematically aligned knee replacements (Howell and Hull, 2012; Theodore et al., 2017) (Table 1). A previously developed MATLAB script (Fitzpatrick et al., 2012) was used to automatically generate surface geometry of the femoral medial and lateral condyles, trochlear and cam geometries, and tibial insert medial and lateral condyles and post geometries from the nine design parameters. The surfaces were meshed as quadrilateral elements, with an average element edge length of 1 mm (Halloran et al., 2005), and a dome-shaped patellar button design was used in all analyses.

Linear and quadratic regression analyses were used to develop the shape-functions within this study. Regression analysis is used to estimate the relationships between multiple predictor variables, or factors, and one or more response variables. There exist many methods of sampling the predictor experimental design space including random, factorial or central-composite, and Latin square designs. Latin hypercube sampling (LHS) allows for sample size selection independent from the number of factors examined. For this study, the models combining design and surgical parameters included 13 factors, which would require 4123 samples to produce

Table 1
Parameter ranges used in training and test data sets for design and surgical parameter sets. Implant geometry was parameterized using nine variables with ranges based on the geometric domain of commercially available TKA components. Six surgical alignment predictors were included, with ranges chosen to capture those of both mechanically and kinematically aligned knee replacements.

Parameter	Low	High
Design Set		
Femoral Distal Radius (mm)	20	50
Femoral Posterior Radius (mm)	20	50
Femoral Coronal Radius (mm)	15	35
Tibial Insert Anterior Conformity	0.15	1.0
Tibial Insert Posterior Conformity	0.15	1.0
Tibial Insert Coronal Conformity	0.15	1.0
Trochlear Groove Angle (degrees)	7.0	17
Trochlear Groove Offset (mm)	−3.0	3.0
Cam Radius (mm)	20	50
Surgical Set (degrees)		
Tibial Insert Vr(+ve)-Vl Alignment	−1.8	7.2
Tibial Insert I(+ve)-E Alignment	−9.4	15.4
Tibial Insert Posterior Slope	0.0	11.2
Femoral Vr(+ve)-Vl Alignment	−0.8	7.2
Femoral I(+ve)-E Alignment	−0.2	5.4
Femoral F(+ve)-E Alignment	0.0	5.0

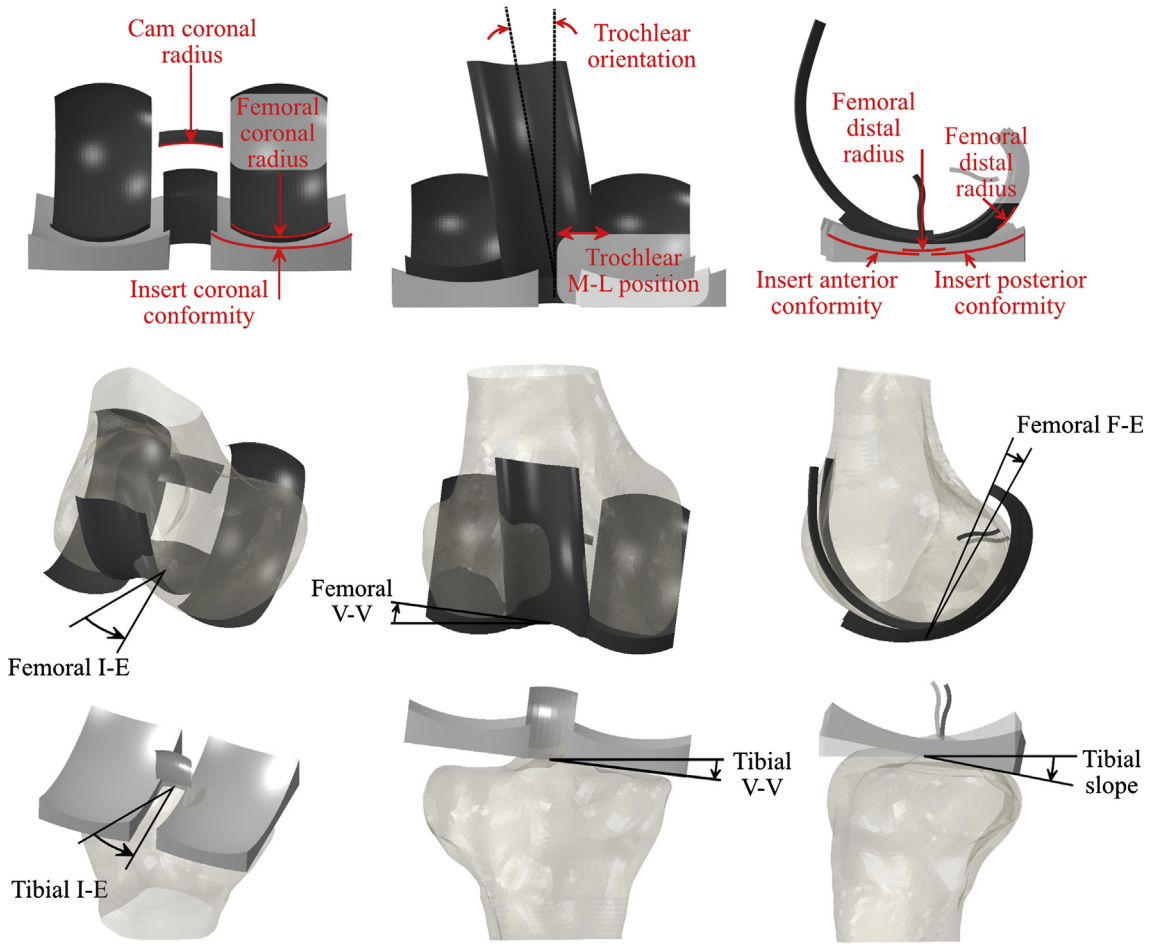

Fig. 2. Design and surgical alignment parameters, with all surgical alignments shown positive. Implant geometry (red) was parameterized using nine variables: femoral condyle distal, posterior and coronal radii, tibial insert anterior, posterior and coronal plane conformity, trochlear orientation and M-L position, and coronal plane curvature of the cam mechanism. Six surgical alignment predictors (black) included: tibial insert and femoral implant V-V and I-E alignment, femoral F-E alignment, and tibial insert slope, with ranges chosen to capture those of both mechanically and kinematically aligned knee replacements. (For interpretation of the references to color in this figure legend, the reader is referred to the web version of this article.)

a 1/6 fractional central composite design. As such, computationally efficient LHS was selected for this study. An initial sample rate of 20 FE simulations per predictor variable was selected, followed by halving the rate to 10 simulations per predictor, to compare the accuracy of predictions with reduced design space sampling.

For the surgical alignment and design parameter combination set, the initial rate of 20 FE simulations per predictor resulted in a sampling of 300 simulations. In order to reduce the computational cost of this set, the two least critical parameters were eliminated. This was accomplished using factor effect screening analysis, which was performed by dividing output results into low and high factor blocks, where each predictor variable was categorized as low when set below its average value, and high when set above average. For every combination of output and input, the magnitude of the difference between the high block and the low block were collected into functional groups of outputs, including: joint loads, contact mechanics, kinematics, and ligament elongations (Table 2). These factor sensitivities were used to populate Pareto charts (Fig. 3), which were used to remove implant F-E surgical alignment and cam radius design parameters from the combined set.

With sets including nine design parameters, six surgical alignments, and a combined set of 13 parameters, the initial sampling rate produced 180, 120, and 260 simulations for the design, surgical, and combined sets, respectively. Following this initial sampling, the half-sized samples produced 90 simulations for the design, 60 for the surgical, and 130 for the combination sets. For all sets of data, linear regression was performed using MATLAB's fitlm function, across all response variables for every increment of time. A DKB was simulated over three seconds with a time increment of 0.025 s, resulting in 121 regression models (1 at each time point) for each response variable. The initial sets of data included enough simulations to allow for regression models specified as having quadratic predictors with interaction terms included (Q + I), but the reduction in simulations for the final set forced the use of linear predictors during the fitting process. To investigate and uncouple sample rate from predictor order, additional data was generated using the large sets with linear predictors, and all half-sized sets using MATLAB's stepwiselm function, which produces linear models using a forward-and-backwards stepwise algorithm. This algorithm uses a residual sum-of-squares criterion for adding or removing terms, and was initialized with linear predictors. Reported response variables were combined into functional groups, including joint loads, contact mechanics, kinematics, and ligament elongations (Table 2).

To quantify the predictive capability of the models for each of design, surgical, and combination sets, 100 additional parameter combinations were generated for each, using randomized parameter values sampled from uniform distributions of each factor range. This number was selected such that the central limit theorem (CLT) would be satisfied by a wide margin. 30 samples are required by the CLT to ensure that calculated RMS error estimations approach their true mean errors. The parameter values were input into each regression model, and the resulting outputs were compared to those of an FE simulation using the same parameters. This comparison was quantified using root mean square (RMS) errors averaged across all randomized test simulations. To measure the relative size of the RMS errors to their respective response variables, the average ranges of 95% confidence intervals for each parameter, and the percentage of the range represented by the RMS errors were reported as average normalized RMS errors.

Table 2
Predicted outputs organized by functional groupings used in factor effect screening. Four groups were created for the tibiofemoral joint, while a single group collected all outputs for the patellofemoral joint.

Functional Group	Response Outputs
Tibiofemoral Joint Loads	A-P force, compressive force, V-V torque, I-E torque
Tibiofemoral Contact Mechanics	Contact area, pressure, and center of pressure
Tibiofemoral Kinematics	A-P translation, I-E rotation, V-V rotation
Ligament Elongations and Muscle Forces	PCL, PMC, MCL, POM, ALC, POL, LCL, and PL elongations; PFL elongation and forces, and vasti muscle force
Patellofemoral Mechanics	M-L, S-I, and A-P contact force; Contact area, pressure, and center of pressure; All clinical translations and rotations, PL elongation and force

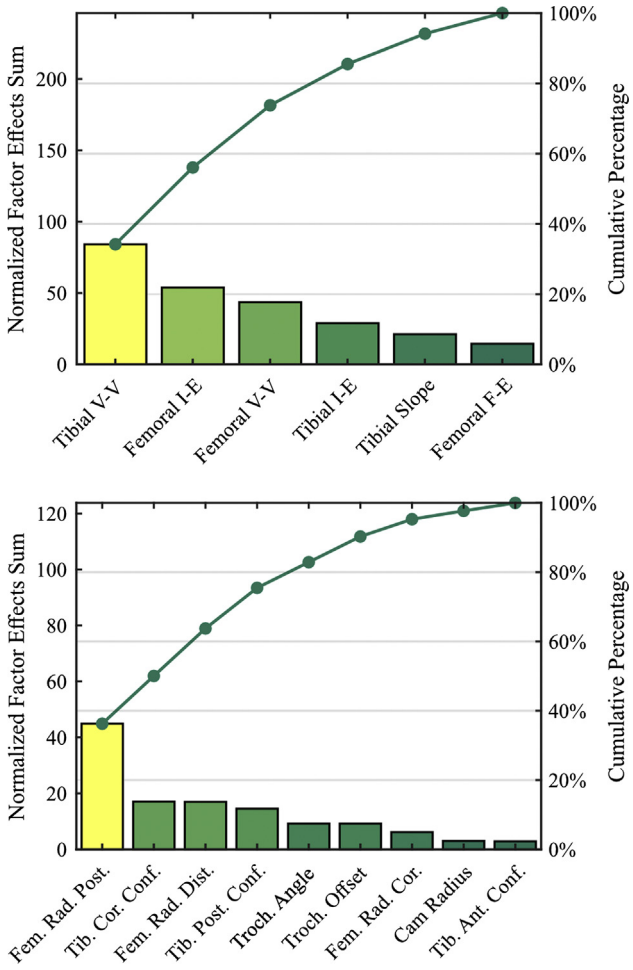

Fig. 3. Pareto charts developed from factor effect screening analysis for the surgical alignment (top) and design (bottom) parameters. Factor effects screening was performed by dividing output results into low and high factor blocks, where each single predictor variable was categorized as low when set below its average value, and high when set above average. For every combination of output and factor, the magnitude of the difference between the high block and the low block was normalized by dividing by the average.

3. Results

DKB predictions were performed for each parameter set, with calculated average normalized RMS errors producing similar trends for each parameter set (Table 3). For the design parameters, when using linear predictors and a rate of 10 samples per parameter, the average normalized RMS error was 7.8%. This error was reduced to 7.4% when doubling the sampling rate, and further reduced to 4.9% when specifying Q + I predictors. The surgical parameter set behaved similarly – average normalized RMS error

Table 3
Average normalized RMS errors for all outputs (%). Across all three parameter sets, doubling the sample rate while using quadratic predictors with interactions reduced errors by an average of 30.1%. Further investigation of sensitivity to predictor order was performed on the design set, due to it having the largest reduction in error with increasing order.

Sample Rate (Simulations/Parameter)		Mean Normalized RMS Error (%)		
	Predictor Order	Surgical	Design	Combined
10	Linear	4.13	7.80	9.42
10	Stepwise Linear	4.13	7.18	9.67
20	Linear	3.99	7.38	8.97
20	Linear with Interactions	–	6.54	–
20	Pure Quadratic	–	6.77	–
20	Quadratic with Interactions	2.79	4.89	7.49

was 4.1% with linear predictors and smaller sample rate, which reduced to 4.0% when doubling the sample rate, and was minimized to 2.8% with increasing predictor order. Combining the design and surgical parameters resulted in an average normalized RMS error of 9.4% when sampled at 10 simulations per parameter using linear predictors. Using 20 simulations per parameter decreased the error to 9.0%, and including Q + I predictors further reduced the average normalized RMS error to 7.5%. Across all parameter sets, doubling the sample rate while using Q + I predictors reduced errors by an average of 30.1%. Due to the considerable gains in computational efficiency and for brevity, only specific output results from the smaller sample size of 10 simulations per parameter using linear predictors are presented here. The design set had 47 out of a total of 56 outputs below 15% normalized RMS error, with the highest error being 25.7%. The surgical set had average normalized RMS errors for nearly all 56 outputs below 15%, with the lone exception of lateral area, which resulted in a predictive error of 16.8%. For the combination set, 43 of the 56 outputs were below 15% average normalized RMS errors, with all errors falling below 28.8%. Results for each parameter set may be specified by functional groups, including: patellar, ligament elongation, kinematics, joint loads, and contact mechanics outputs (Fig. 4). Key results for individual sets are detailed below.

3.1. Patella

Patellofemoral kinematics, contact mechanics and joint forces represented one functional group. For this group, mean normalized RMS errors, averaged by group, were below 5% across all parameter sets, with errors of 2.4%, 3.6%, and 4.2% for surgical, design, and combined sets, respectively. For the surgical set, every output scored a mean normalized RMS error below 5%, while both the design and combination set included error terms below 10%, except for the M-L center of pressure, at 10.2% and 10.8% for the design and combined sets, respectively. A-P and S-I rotation, M-L and compressive A-P contact forces were accurately predicted, with mean normalized RMS errors below 2.5% for all parameter sets.

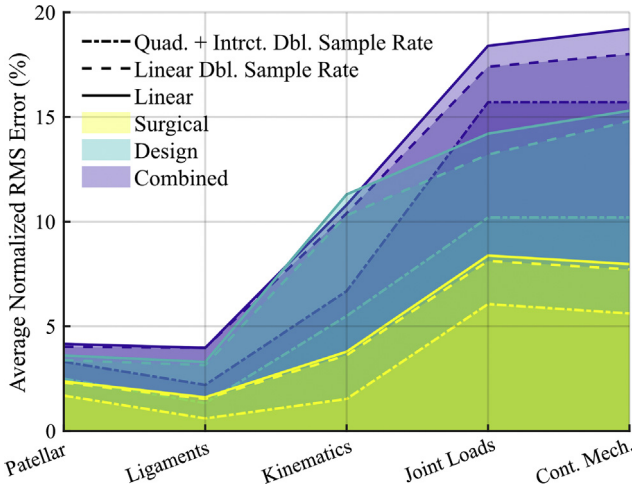

Fig. 4. Overlayed area plots of average normalized RMS error by functional group. Within each set of parameters, highest errors are associated with linear predictors using half-sized sample rates, and are reduced by keeping linear predictors while doubling the sampling rate, then minimized using doubled sample rate with quadratic predictors with interaction terms. Joint loads and contact mechanics functional groups produced larger differentiation between each set, with the small sample rate with linear predictor sets showing average differences in errors of 5.6% and 5.0% when going from surgical to design, and design to combination sets, respectively.

3.2. Ligament elongation and muscle forces

The ligament group included MCL, LCL, PFL, PMC, POM, POL, and ALC elongations and vasti and PFL forces. The remaining forces developed in the ligaments were omitted due primarily to large domains of inactivity during the DKB; only a small subset of geometries produced forces, skewing all predictions for these omitted outputs. This group also had normalized mean RMS errors, averaged by group, below 5% across all parameter sets, with errors resulting in 1.6%, 3.3%, and 4.0% for the surgical, design, and combined sets, respectively. For the combined set, the highest mean normalized RMS error resulted from MCL elongation at 8.8%. Prediction of forces developed within the PFL resulted in an error of 4.2%, while vasti muscle force predictions contained an error of 3.2% (Fig. 5).

3.3. Tibiofemoral kinematics

Kinematics predictions of the TF joint resulted in normalized mean RMS errors, averaged by group, of 3.8% for the surgical, 11.3% for the design, and 10.8% for the combination parameter sets. For the surgical set, all mean normalized RMS errors were less than 6.3%. All outputs of the design set, apart from M-L translation, fell below a mean normalized RMS error of 11%. The design set exception, M-L translation, had an error of 25.7%. For the combination set, predicted mean normalized RMS errors for S-I and A-P translations, and V-V rotation fell below 10%, while M-L translation and I-E rotation had prediction errors of 15.5% and 19.0%, respectively (Fig. 6).

3.4. Tibiofemoral joint loads

The TF joint loads functional group contained eight outputs, including: A-P and compressive forces, as well as V-V and I-E torques for both medial and lateral condyles of the tibial implant. For the surgical set, normalized mean RMS joint load errors, averaged by group, were only 8.4%, whereas the design set resulted in an error of 14.2%, and the combined set had the largest error of 18.4% for this group. For the combination set, all contact forces were predicted with mean normalized RMS errors less than 15% except for the medial A-P joint force, which scored 20.5% (Fig. 7). At the other end of the range, medial and lateral tibial insert joint

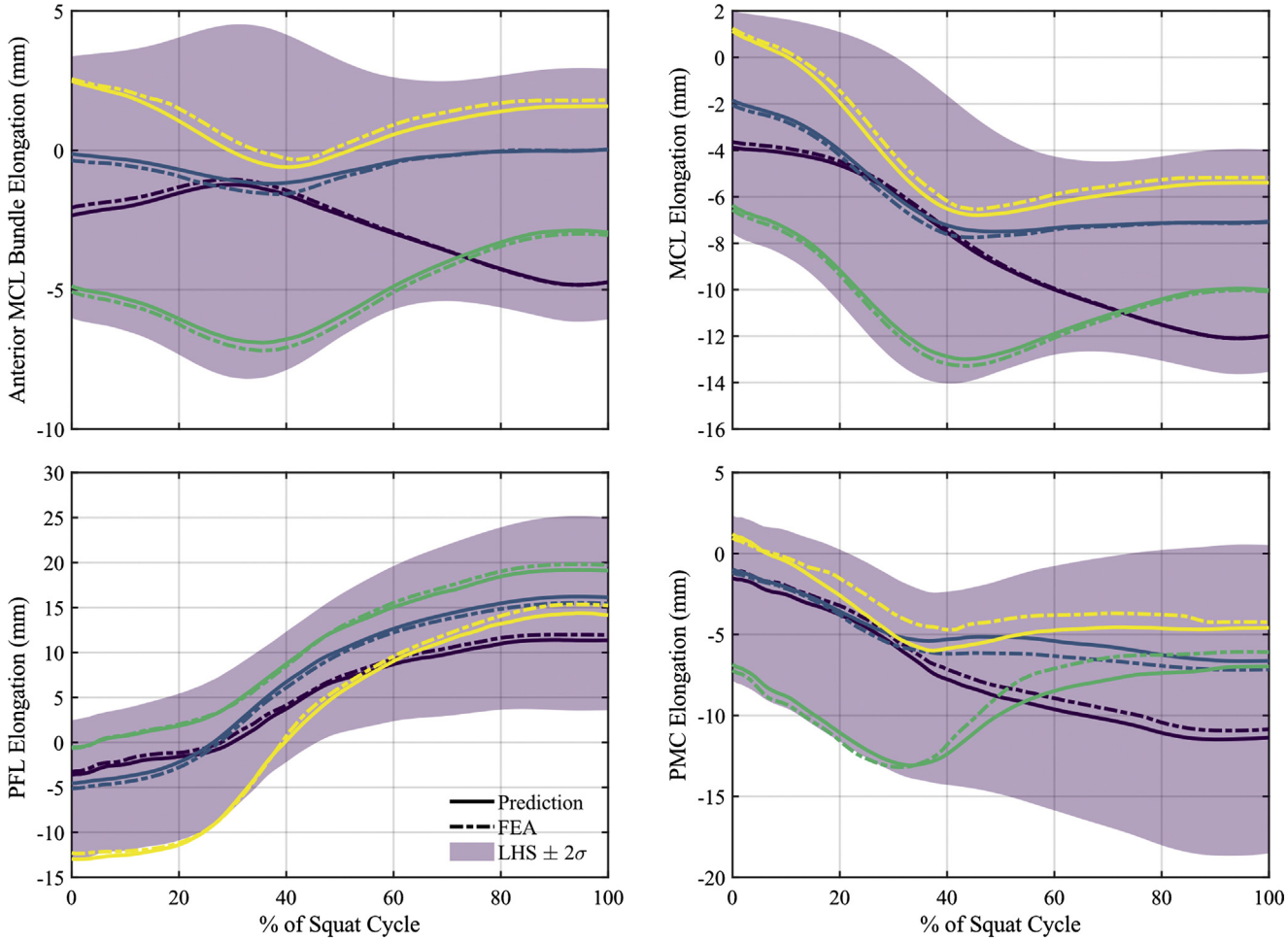

Fig. 5. Select results from the ligament elongation functional group, from the combination test set using a LHS sample size of 130 simulations with linear predictors. This functional group had normalized mean RMS errors, averaged by group, below 5% across all parameter sets, with errors resulting in 1.61%, 3.30%, and 3.97% for the surgical, design, and combined sets, respectively.

torques scored mean normalized RMS errors between 21.3% and 28.8%.

3.5. Contact mechanics

The contact mechanics functional group included contact areas and pressures, and center of pressure locations in the S-I, M-L, and A-P directions, from both the medial and lateral condyles. For these 10 outputs, the surgical set had a normalized mean RMS error, averaged by group, of 8.0%, while the design set scored 15.3%, and the combination set resulted in an error of 19.2%. For the surgical set, all mean RMS errors were below 15%, except for contact area on the lateral side of the tibial insert at 16.8%. For the design set, contact pressures and their A-P locations were within mean normalized RMS errors of 7.9%, with the remaining outputs falling between 15.3% and 24.2%. For the combination set, contact pressures and A-P locations fell below mean normalized RMS errors of 13.4%, with the rest of the error terms falling between 20.2% and 28.2% (Fig. 7).

4. Discussion

The goal of this study was to generate a statistical model to predict contact mechanics and kinematic outcomes of the TKA joint during a DKB activity due to implant design and surgical alignment. Utilizing a set of five surgical alignment and eight implant geometry parameters, our most computationally efficient model (130 training FE simulations) is able to instantaneously predict outputs relating to patellar, ligament elongations, and kinematics functional groups with high precision, resulting in errors less than 12%. Our model is also able to predict outputs from the contact mechanics and joint loads functional groups with an aggregate mean normalized RMS error below 20%, and we have quantified the reduction in error as the result of doubling sample size and increasing predictor order.

While it was expected that the joint loads and contact mechanics functional groups would prove the most challenging to predict, it was interesting that the average normalized RMS error of the kinematics group was reduced when moving from the design to combination parameter sets. Furthermore, when increasing the predictor order to include Q + I terms, the largest reductions in error, 4.1% for the combination and 5.8% for the design sets, came from the kinematics functional group. These results suggest that the relationship between knee kinematics and design parameters may exhibit more nonlinearity than the other functional groups. It may be beneficial for future studies where kinematic prediction is critical to use sample sizes large enough for Q + I predictors in the regression models.

For each parameter set within this study, FE simulations were performed in order to train the statistical model for two different sampling rates. Additionally, test simulations were also run to quantify the accuracy of the shape-function model predictions.

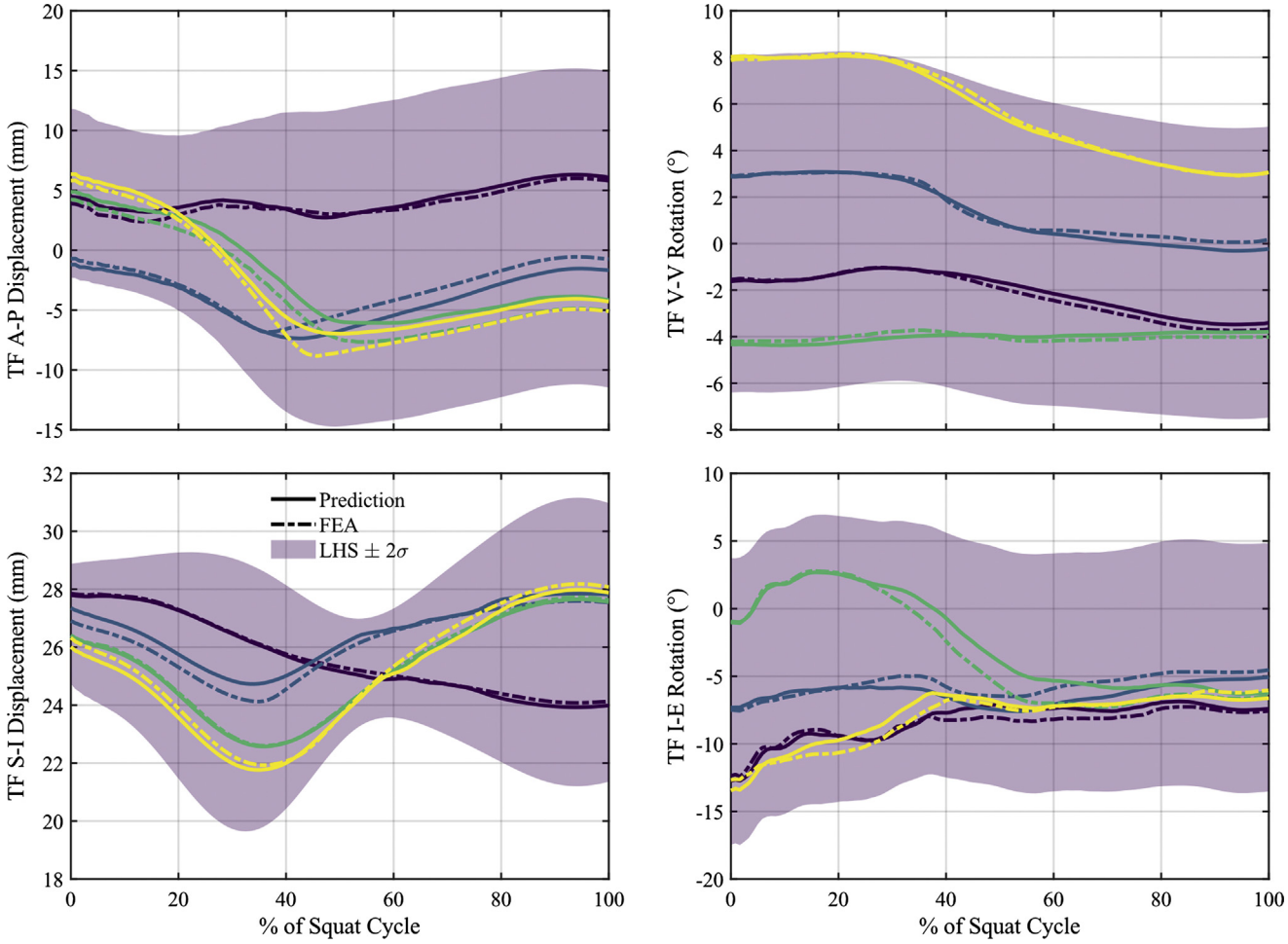

Fig. 6. Prediction of kinematic results for tibiofemoral A-P and S-I displacement, and I-E and V-V rotation of the combination parameter set using 10 simulations per parameter with linear predictors. Kinematics predictions of the TF joint resulted in normalized mean RMS errors, averaged by group, of 3.78% for the surgical, 11.3% for the design, and 10.8% for the combination parameter sets.

Due to these requirements, over 1000 simulations were performed which necessitated a computationally efficient knee model, and a number of assumptions and simplifications were required. The removal of F-E surgical alignment and cam radius parameters in the combined set was based on factor-effect screening, and these results are likely activity-specific – a different activity may affect the relative influence of these parameters. The model created a physiological loading condition at the knee joint, but not in a perfectly physiological fashion. Only the quadriceps muscle was included, with net contribution from the rest of the muscles incorporated without direct representation. The vertical hip load primarily controlled the compressive load at the joint, the A-P force at the joint was controlled by application of an A-P force to the femur, and I-E and V-V torques were controlled by moments applied to the tibia. The loading condition represented in the FE model reflects a single knee flexion activity. While we have made efforts to ensure that this loading condition is a valid representation of kinematics and joint loads from a TKA patient performing this activity, there is likely wide variability in loads across the TKA population which have not been accounted for in this model. However, the shape function modeling framework presented in this study could be expanded to include easily measurable patient-specific parameters (e.g. weight, limb alignment, lower limb mechanics, etc.) in order to develop a SFM that can be customized to an individual patient.

In the current study, the bounds of the parameters included in our analysis are guided by current design and alignment strategies, and our predictions have only been validated within these bounds. To investigate a broader range of design and alignment parameter would likely require development of a new SFM which incorporated these extended ranges in the training set. We would expect our current model to perform well with small deviations outside our current ranges, but would likely have poorer performance with large deviations, particularly with combinations of parameters that may result in discontinuities in joint mechanics behavior such as edge loading or joint dislocation. An additional constraint of the shape-function model developed in this study is that is has been developed to predict results from finite element simulations, rather than in vivo data. However, as finite element simulation is becoming increasingly used and accepted in pre-clinical design phase of prospective devices, the approach described here has distinct benefit in reducing the time and computational resources required during this iterative phase.

The present framework could be utilized for implant design in an optimization pipeline such as that used by Willing and Kim (2011, 2012). These studies utilized single and multi-objective optimization methods to solve for an optimized design based on minimizing deviation from natural knee kinematics. Performing optimization using these techniques required iteratively solving of the objective function hundreds of times in order to minimize deviation from natural knee laxity data. Each solution of this function required an FE simulation, and the computational requirements to perform one entire optimization were reported as 10 days of calculations for one of these studies. Comparatively,

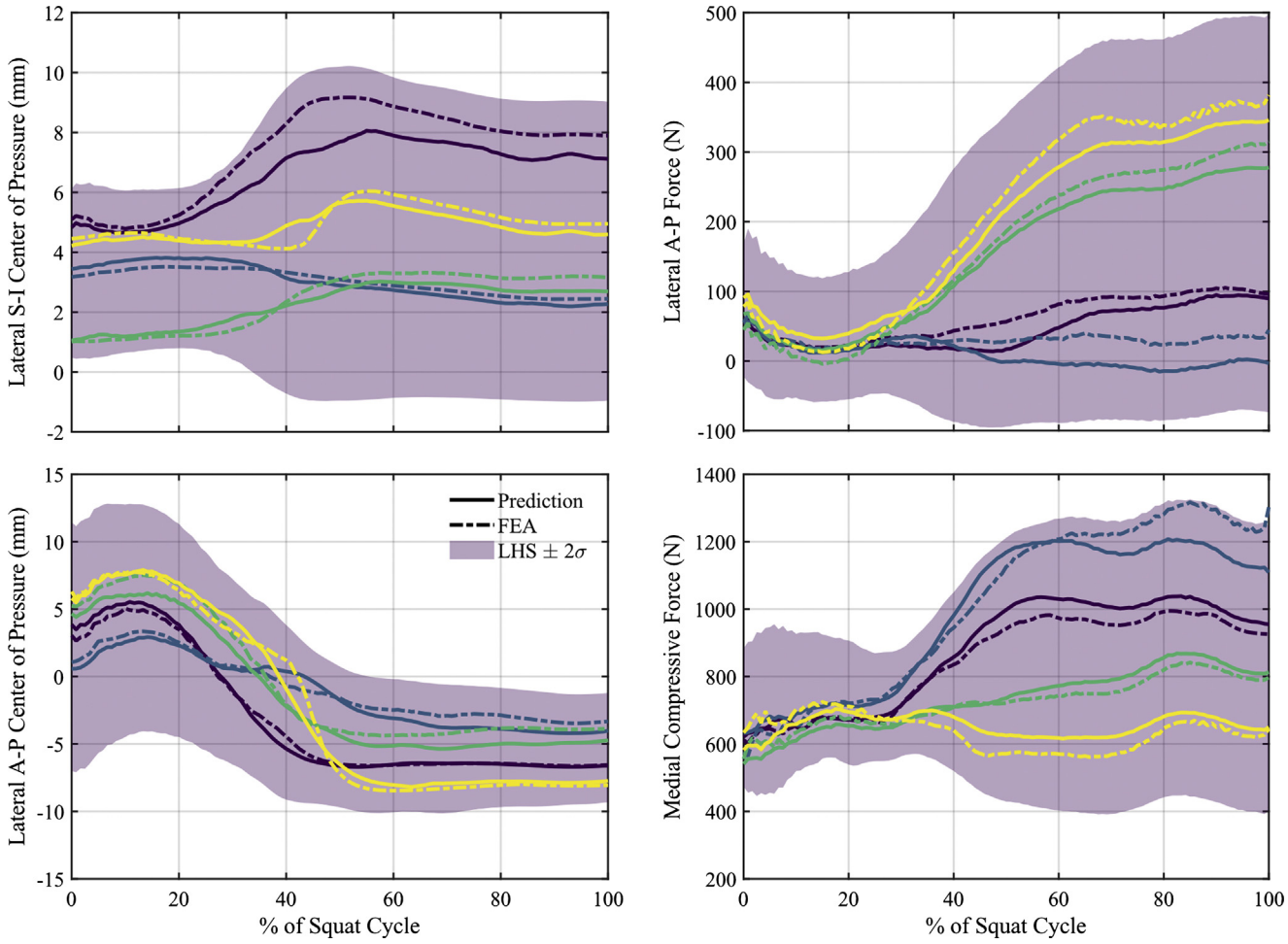

Fig. 7. Representative contact mechanics and joint loads prediction results from the combination set, using a sample size of 130 simulations and linear predictors for regression analysis. From the contact mechanics group, the surgical set had a normalized mean RMS error, averaged by group, of 8.0%, while the design set scored 15.3%, and the combination set resulted in an error of 19.2%. For the surgical set, normalized mean RMS joint load errors, averaged by group, were only 8.38%, whereas the design set resulted in an error of 14.2%, and the combined set had the largest error of 18.4% for this group.

the up-front computational cost to build the statistical SFM was 130 simulations, with each simulation taking 20 min to solve on a standard PC using a single CPU, for an initial time-savings of eight days. Once produced, the SFMs developed in this study are able to predict all output results from a simulation nearly instantaneously within a high degree of accuracy, resulting in computational requirements to produce a similar number of results measured in seconds, not days.

This work illustrates the efficacy of statistical models in pre-clinical design of TKA devices. The SFM generated instantaneous joint mechanics predictions using a small number of training simulations, making it ideally suited for integration into a design optimization pipeline. Such a tool may be used, for example, to optimize kinematic function to achieve more natural kinematics or minimize implant wear. Additionally, patient-specific parameters, such as limb alignment and weight, could be included in a similar optimization pipeline and integrated into surgical planning tools to guide clinicians in choosing alignments that optimize joint mechanics and kinematics outcomes. These tools may aid the engineering and clinical communities in improving patient satisfaction and surgical outcomes.

Conflict of interest statement

There are no conflicts of interest in this project from any of the authors.

References

Ardestani, M.M., Moazen, M., Jin, Z., 2015. Contribution of geometric design parameters to knee implant performance: conflicting impact of conformity on kinematics and contact mechanics. Knee, 217–224.
Baldwin, M.A., Clary, C.W., Fitzpatrick, C.K., Deacy, J.S., Maletsky, L.P., Rullkoetter, P. J., 2012. Dynamic finite element knee simulation for evaluation of knee replacement mechanics. J. Biomech., 474–483.
Choi, Y.-J., Ra, H.J., 2016. Patient satisfaction after total knee arthroplasty. Knee Surg. Relat. Res., 1–15.
Dhaher, Y.Y., Kahn, L.E., 2002. The effect of vastus medialis forces on patello-femoral contact: a model-based study. J. Biomech. Eng., 758–767.
Elias, J.J., Kilambi, S., Cosgarea, A.J., 2010. Computational assessment of the influence of vastus medialis obliquus function on patellofemoral pressures: model evaluation. J. Biomech., 612–617.
Farahmand, F., Tahmasbi, M.N., Amis, A., 2004. The contribution of the medial retinaculum and quadriceps muscles to patellar lateral stability. Knee, 89–904.
Fitzpatrick, C.K., Clary, C.W., Rullkoetter, P.J., 2012. The role of patient, surgical, and implant design variation in total knee replacement performance. J. Biomech., 2092–2102.
Fitzpatrick, C.K., Baldwin, M.A., Clary, C.W., Maletsky, L.P., Rullkoetter, P.J., 2014. Evaluating knee replacement mechanics during ADL with PID-controlled dynamic finite element analysis. Comput. Methods Biomech. Biomed. Eng. 17 (4), 360–369.
Galloway, F., Worsley, P., Stokes, M., Nair, P., Taylor, M., 2012. Development of a statistical model of knee kinetics for applications in pre-clinical testing. J. Biomech., 191–195.
Godest, A.C., Beaugonin, M., Haug, E., Taylor, M., Gregson, P.J., 2002. Simulation of a knee joint replacement during a gait cycle using explicit finite element analysis. J. Biomech., 267–275.
Hashemi, A., Shirazi-Adl, A., 2000. Finite element analysis of tibial implants – effect of fixation design and friction model. Comput. Methods Biomech. Biomed. Eng. 3 (3), 183–201.

Halloran, J.P., Petrell, A.J., Rullkoetter, P.J., 2005. Explicit finite element modeling of total knee replacement mechanics. J. Biomech., 323–331.
Heinlein, B., Graichen, F., Bender, A., Rohlmann, A., Bergman, G., 2007. Design, calibration and pre-clinical testing of an instrumented tibial tray. J. Biomech. 40, S4–S10.
Howell, S.M., Hull, M.L., 2012. Kinematic alignment in total knee arthroplasty. In: Insall and Scott Surgery of the Knee. Elsevier, pp. 1255–1268.
Kessler, O., Patil, S., Colwell Jr, C.W., D'Lima, D.D., 2008. The effect of femoral component malrotation on patellar biomechanics. J. Biomech., 3332–3339.
Kutzner, I., Heinlein, B., Graichen, F., Bender, A., Rohlmann, A., Halder, A., Beier, A., Bergmann, G., 2010. Loading of the knee joint during activities of daily living measured *in vivo* in five subjects. J. Biomech. 43, 2164–2173.
Mesfar, W., Shirazi-Adl, A., 2005. Biomechanics of the knee joint in flexion under various quadriceps forces. Knee, 424–434.
Scuderi, G.R., Bourne, R.B., Noble, P.C., Benjamin, J.B., Lonner, J.H., Scott, W.N., 2012. The new knee society knee scoring system. Clin. Orthop. Relat. Res., 3–19.
Theodore, W., Twiggs, J., Kolos, E., Roe, J., Fritsch, B., Dickison, D., Liu, D., Salmon, L., Miles, B., Howell, S., 2017. Variability in static alignment and kinematics for kinematically aligned tka. Knee, 733–744.
Thompson, J.A., Hast, M.W., Granger, J.F., Piazza, S.J., Siston, R.A., 2011. Biomechanical effects of total knee arthroplasty component malrotation: a computational simulation. J. Orthop. Res., 969–975.
Willing, R., Kim, I.Y., 2011. Design optimization of a total knee replacement for improved constraint and flexion kinematics. J. Biomech., 1014–1020.
Willing, R., Kim, I.Y., 2012. Quantifying the competing relationship between durability and kinematics of total knee replacements using multiobjective design optimization and validated computational models. J. Biomech., 141–147.